Volume 1 | Number 1 | Jan 2013 | Pages 1–100

PCCP

Physical Chemistry Chemical Physics
www.rsc.org/pccp

ROYAL SOCIETY OF CHEMISTRY

This is an *Accepted Manuscript*, which has been through the Royal Society of Chemistry peer review process and has been accepted for publication.

Accepted Manuscripts are published online shortly after acceptance, before technical editing, formatting and proof reading. Using this free service, authors can make their results available to the community, in citable form, before we publish the edited article. We will replace this *Accepted Manuscript* with the edited and formatted *Advance Article* as soon as it is available.

You can find more information about *Accepted Manuscripts* in the **Information for Authors**.

Please note that technical editing may introduce minor changes to the text and/or graphics, which may alter content. The journal's standard **Terms & Conditions** and the **Ethical guidelines** still apply. In no event shall the Royal Society of Chemistry be held responsible for any errors or omissions in this *Accepted Manuscript* or any consequences arising from the use of any information it contains.

A Computational Study of Doped Olivine Structured Cd$_2$GeO$_4$: Local Defect Trapping of Interstitial Oxide Ions[†]

Adam J. McSloy,[a] Paul F. Kelly,[a] Peter R. Slater[b] and Pooja M. Panchmatia[*a]

Computational modelling techniques have been employed to investigate defects and ionic conductivity in Cd$_2$GeO$_4$. We show due to highly unfavourable intrinsic defect formation energies the ionic conducting ability of pristine Cd$_2$GeO$_4$ is extremely limited. The modelling results suggest trivalent doping on the Cd site as a viable means of promoting the formation of the oxygen interstitial defects. However, the defect cluster calculations for the first time explicitly suggest a strong association of the oxide defects to the dopant cations and tetrahedral units. Defect clustering is a complicated phenomenon and therefore not trivial to assess. In this study the trapping energies are explicitly quantified. The trends are further confirmed by molecular dynamic simulations. Despite this, the calculated diffusion coefficients do suggest an enhanced oxide ion mobility in the doped system compared to the pristine Cd$_2$GeO$_4$.

1 Introduction

In the search for new oxide ion conductors, perovskite, fluorite and apatite type materials have been the focus of most investigations due to their fast oxide ion conducting abilities.[1] Although such materials are promising, many different structural classes remain as yet uninvestigated. The oxygen-rich apatite-type conductors differ from most in that ionic conduction occurs *via* a faster interstitial mechanism rather than a vacancy mechanism.[2] Fast interstitial oxide conduction is often observed in oxygen excess materials which possess flexible tetrahedral frameworks, such as apatites or melilites.[2–6] As a result of this one could envisage that structures with similar frameworks capable of accommodating interstitial oxide ions may also present fast ionic conductivities. One such material is cadmium orthogermanate (Cd$_2$GeO$_4$) which is of interest due to its structural similarity to the apatites in that it possesses isolated tetrahedra and so may be prone to interstitial formation *via* either isolated interstitial oxide ion defects, or by increasing the coordination sphere of Ge, as in the apatite systems, and hence showing enhanced ionic conductivity. Its olivine structure is also of interest since Li-containing olivines have been shown to be good ionic conductors, albeit Li

ions conductors *via* a vacancy mechanism.[7] Still, this material's open structure does warrant further investigation as a potential oxide ion conductor.

Cadmium orthogermanate, of the formula Cd$_2$GeO$_4$, crystallises with an orthorhombic olivine type *Pmcn* structure. As shown in figure 1 the Cd ions occupy two distinct lattice sites. The O ions coordinate octahedrally to the Cd ions and tetrahedrally to the Ge ions. The isolated GeO$_4$ groups form channels down the *b-axis* and are spaced both vertically and horizontally by channels of Cd$_I$ and Cd$_{II}$ ions. To date, there is no literature on the applications of Cd$_2$GeO$_4$ as a solid oxide fuel cell (SOFC) material, however Whipple *et al.* reported the semiconducting properties for Cd$_2$GeO$_4$ in the 80's.[8] They found that conductivity is enhanced when doping with trivalent metal ions for samples heated under a vacuum, where they suggested that the electrons originate from shallow donors with their mobility determined by a combination of large polaron formation and impurity scattering. They also reported a large drop in electrical conductivity is observed upon exposure to oxygen which is thought to originate from the reversible chemisorption of oxygen on to the surface of the grains.

2 Computational Methodology

The simulation methods employed in this study are reviewed in brief here, but more comprehensive reviews can be found elsewhere.[9–11] Interatomic potential based energy minimisation calculations were performed using the general utility lattice program (GULP)[12,13] and molecular dynamics simulations using

[a] *Department of Chemistry, Loughborough University, Loughborough LE11 3TU, United Kingdom.*

[b] *School of Chemistry, The University of Birmingham, Edgbaston, Birmingham B15 2TT, United Kingdom.*

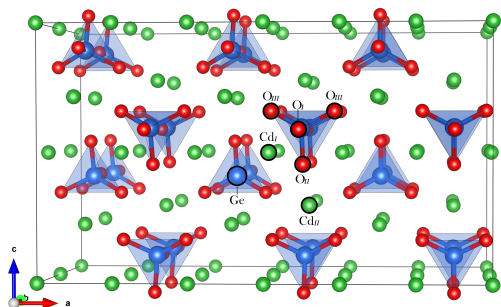† Electronic Supplementary Information (ESI) available: See DOI: 10.1039/b000000x/

Fig. 1 Structure of Cd_2GeO_4 with Ge, Cd and O ions represented as blue, green and red spheres respectively and GeO_4 tetrahedra in blue.

Table 1 Interatomic potential and shell model parameters for Cd_2GeO_4.

(a) Buckingham potential parameters[†].

Interaction	A (eV)	ρ (Å)	C (eV Å^6)	Ref.
Cd^{2+} - O^{2-}	1207.70	0.327100	0.00	-
Ge^{4+} - O^{2-}	1497.40	0.325646	16.00	[21]
O^{2-} - O^{2-}	22764.30	0.149000	27.89	[22]

(b) Shell parameters.

Ion	Shell Charge (e)	k (eV Å^{-2})	Ref.
O^{2-}	-2.86	74.92	[22]

[†] A short range potential cut-off of 12 Å was enforced in all static-lattice calculations.

DL_POLY classic[14]. Images in this paper were generated using VESTA visualisation software.[15]

Calculations were based on the Born model for ionic solids where ionic interactions are described using a long range coulombic term and an analytical function representing the short-range Pauli repulsion and attractive van der Waals interactions. In this work the short-range interactions were described with the Buckingham potential[16]:

$$\Phi_{ij}\left(r_{ij}\right) = A\exp\left(-\frac{r_{ij}}{\rho}\right) - \frac{C}{r_{ij}^6} \tag{1}$$

Where Φ_{ij} is the potential energy resulting from the interaction between ions i and j at a distance of r. A, ρ and C are the empirically derived potential parameters specific to each interaction. Potentials from various literature sources were screened to identify a preliminary potential set. These potentials were then empirically fitted to the experimental structure with a high degree of agreement.[17] The interatomic potentials where then further vetted in their respective binary oxides. The final interatomic potentials are presented in table 1. Potentials selected to model the dopants, discussed later, were verified by testing them in their respective binary oxides with the oxide potential listed in table 1a. The electronic polarisability of the ions, which is of particular importance when considering charged defects, was described using the Dick and Overhauser shell model.[18] Point defects were modelled using the Mott Littleton method.[19] This method partitions the area surrounding the defect into two spherical regions. Ions in the central region, which immediately surround the defect, are treated explicitly. While those in the outer region are handled more approximately by quasi-continuum methods.[19] For single-defect calculations the central region's radius was truncated at 12 Å, but this was increased appropriately for larger multi-defect systems. The aforementioned methods have, previously, been successfully employed to model defects in olivine-$(Fg/Mg)_2SiO_4$, $LiFePO_4$ and apatite structures.[5,7,20]

Molecular dynamic (MD) simulations were performed on 5×5×5 supercells containing $\sim$ 3500 ions, at four temperatures 873, 1073, 1273 and 1473 K. Systems were equilibrated at zero kelvin before simulating for a further 3 ns under isothermal-isobaric (NPT) conditions. Final production runs were carried out under constant volume (NVT) conditions for 3 ns with a time step of 0.5 fs. Oxygen shells were included *via* the adiabatic shell model. Diffusion coefficients (D) were derived from the mean squared displacements (MSD), $\langle[\Delta\vec{r}(t)]^2\rangle$, using equation 2. Migration activation energies were then extracted using the Arrhenius relation.

$$D = \frac{MSD}{6t} \tag{2}$$

3 Results and Discussion

3.1 Structural Modelling and Intrinsic Defects

Cd_2GeO_4, shown in figure 1, is an olivine *Pmcn* structured material comprised of Ge tetrahedra and two inequivalent Cd octahedra. In Cd_2GeO_4, the isolated tetrahedra are linked by corner and edge sharing Cd octahedra. These tetrahedra align to form columns down the *b-axis*.

A comparison of the calculated and experimental lattice parameters, table 2a, indicates a good fit to within 1%.[17] Similarly, the interatomic distances, table 2b, are also in reasonable agreement with the experimental data. Such agreement, between the simulated and experimental structures, supports the validity of the model employed in this work.

In materials such as $Ba_2In_2O_4$ the oxygen defects, pivotal to oxide ion conduction, form naturally though oxygen Frenkels.[23,24] However, the formation of Frenkel and Schottky defects in Cd_2GeO_4 is found to be energetically unfavourable therefore the concentration of these defects will be negligibly small even at higher temperatures, listed in table 3. We are confident that the high intrinsic defect energies are not as a result of the interatomic potentials employed since the scrutiny employed to verify the potentials was stringent and included verifying the potentials against the respective binary oxides as well as the integrated properties of the crystal structure such as the interatomic distances and the coordination about each ion among others. As the spontaneous formation of oxygen defects in pristine Cd_2GeO_4 is unfavourable doping was employed to induce their formation.

Table 2 Calculated and experimental properties of Cd$_2$GeO$_4$.[17]

(a) Lattice parameters

Parameter	Calculated	Experimental	Difference (%)
a (Å)	6.528	6.584(3)	-0.056 (-0.86)
b (Å)	5.262	5.211(2)	0.051 (0.98)
c (Å)	11.177	11.160(4)	0.017 (0.16)
$\alpha = \beta = \gamma$ (°)	90.0	90.0	0.0 (0.00)

(b) Interatomic distances (Å)

Bond	Calculated	Experimental	Difference
Cd$_I$ - O$_{II}$ (×2)	2.30	2.29	0.00
Cd$_I$ - O$_I$ (×2)	2.26	2.30	-0.04
Cd$_I$ - O$_{III}$ (×2)	2.40	2.36	0.04
Cd$_{II}$- O$_{II}$	2.23	2.25	-0.03
Cd$_{II}$- O$_{III}$ (×2)	2.25	2.28	-0.03
Cd$_{II}$- O$_I$	2.44	2.36	0.08
Cd$_{II}$- O$_{III}$ (×2)	2.49	2.43	0.06
Ge - O$_I$	1.73	1.76	-0.03
Ge - O$_{III}$ (×2)	1.75	1.76	-0.01
Ge - O$_{II}$	1.77	1.77	0.00

Table 3 Calculated Cd$_2$GeO$_4$ intrinsic defect energies.

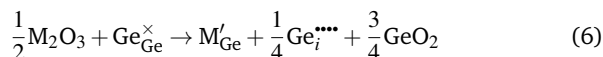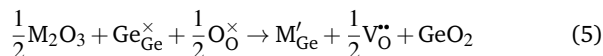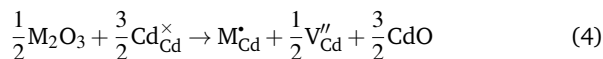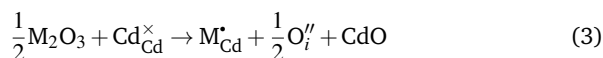| Defect	Defect equation^a	Defect energy (eV)
Cd Frenkel	$Cd_{Cd}^{\times} \rightarrow V_{Cd}'' + Cd_i^{\bullet\bullet}$	6.00
Ge Frenkel	$Ge_{Ge}^{\times} \rightarrow V_{Ge}'''' + Ge_i^{\bullet\bullet\bullet\bullet}$	19.31
O Frenkel	$O_O^{\times} \rightarrow V_O^{\bullet\bullet} + O_i''$	6.25
Schottky	$2Cd_{Cd}^{\times} + Ge_{Ge}^{\times} + 4O_O^{\times} \rightarrow$	31.41
	$\quad 2V_{Cd}'' + V_{Ge}'''' + 4V_O^{\bullet\bullet} + Cd_2GeO_4$	

^{a} Equations given in Kröger-Vink notation.

3.2 Doping

Aliovalent doping is a well-known method of promoting oxygen defect formation in oxide materials.[1,25] During the course of investigation a broad range of mono, di, tri and tetravalent dopant ions on both cation sites were investigated. Considering both constant-cation and constant-oxygen based methods of charge-compensation. In constant-cation mechanisms, such as equations 3 and 5, charge-compensation is achieved through the formation of oxygen interstitials or vacancies. While constant-oxygen mechanisms are charge balanced by cation vacancies or interstitials, as seen in equations 4 and 6. The relative favourability of a particular dopant and its incorporation pathway can be established from its solution energy, which is calculated from its constituent isolated point defect energies and relevant lattice energies. Investigations concluded that constant-oxygen stoichiometry was favoured in all but the trivalent doping mechanisms. This suggests that mono, di, and tetravalent doping would primarily result in the formation of cation defects, rather than oxide defects. As these mechanisms do not offer a means to induce oxygen defect formation they are considered no further.

In this work four different trivalent doping mechanisms were considered. The first two, shown in equations 3 and 4, represent trivalent doping of the Cd sites (M$_{Cd}^{\bullet}$). With the charges in the former and latter compensated by O interstitial (O$_i''$) and Cd va-

cancy (V$_{Cd}''$) defects respectively. The oxygen vacancy (V$_O^{\bullet\bullet}$) and Ge interstitially (Ge$_i^{\bullet\bullet\bullet\bullet}$) compensated Ge site doping (M$_{Ge}'$) mechanisms are represented in equations 5 and 6 correspondingly.

$$\frac{1}{2}M_2O_3 + Cd_{Cd}^{\times} \rightarrow M_{Cd}^{\bullet} + \frac{1}{2}O_i'' + CdO \tag{3}$$

$$\frac{1}{2}M_2O_3 + \frac{3}{2}Cd_{Cd}^{\times} \rightarrow M_{Cd}^{\bullet} + \frac{1}{2}V_{Cd}'' + \frac{3}{2}CdO \tag{4}$$

$$\frac{1}{2}M_2O_3 + Ge_{Ge}^{\times} + \frac{1}{2}O_O^{\times} \rightarrow M_{Ge}' + \frac{1}{2}V_O^{\bullet\bullet} + GeO_2 \tag{5}$$

$$\frac{1}{2}M_2O_3 + Ge_{Ge}^{\times} \rightarrow M_{Ge}' + \frac{1}{4}Ge_i^{\bullet\bullet\bullet\bullet} + \frac{3}{4}GeO_2 \tag{6}$$

The calculated solution energies for the trivalent doping of Cd$_2$GeO$_4$ at the Cd$_{II}$ and Ge sites, following equations 3-6, are plotted in figure 2 as a function of dopant ionic radii. It should be noted that 6 coordinate radii have been used in figure 2 to aid comparison, and that radii for the high-spin states have been used where applicable. Results show Cd, specifically Cd$_{II}$, site substitution mechanisms are favoured by all but the smallest trivalent dopant ion tested (Al), which is consistent with experimental suggestions.[8,26] The larger dopants, such as La, are favoured as their ionic radii are closer to Cd (0.95 Å), making them more appropriate.[27] The results show that Ge based substitution are generally unfavourable, with high defect energies. Substitutions on the Cd site are predicted to be more favourable, with a small preference for constant-cation stoichiometry in which charge compensating oxygen interstitials form. This indicates that trivalent doping offers a potential method of forming oxygen interstitial defects.
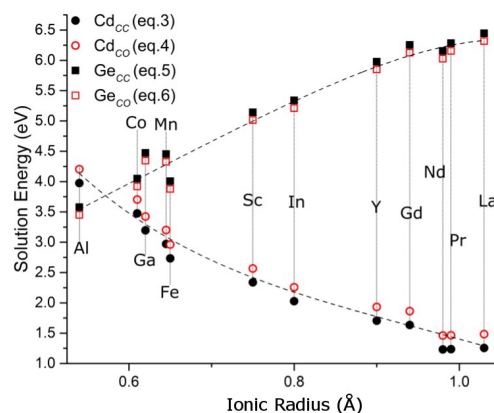
Fig. 2 Solution energies for M^{3+} doping of the Cd$_{II}^{2+}$ and Ge^{4+} sites *via* mechanisms 3 (Cd$_{CC}$), 4 (Cd$_{CO}$), 5 (Ge$_{CC}$) and 6 (Ge$_{CO}$).

3.3 Defect Clustering

It is known that defects, particularly those of opposite charge, generally tend to associate with one another.[28] These defect-defect interactions, which are determined by coulombic forces and lattice relaxations, can significantly affect defect mobility and could result in ion trapping.[29,30] Although in general one would expect that introducing a trivalent dopant on the Cd site giving rise to donor defects of opposite charge should result in

some level of clustering, it has been shown many a times that ionic conductivity is significantly enhanced in e.g. apatites[2,31] and little of evidence of defect trapping is observed. Therefore, an understanding of clustering behaviour will be important in understanding material stability, and offer insight into ionic conductivity thus aiding the dopant selection process. For this, $2M^{\bullet}_{Cd}{:}O''_i$ defect clusters, where M = Sc^{3+}, Y^{3+}, Nd^{3+}, Pr^{3+} and La^{3+}, were examined. The lanthanides were considered due to their large sizes and low incorporation energies. The two comparatively smaller dopants Y and Sc were also included to elucidate the effects of dopant size on defect clustering, and due to existence experimental data for the former.[8]

The identification of stable conformations is an important consideration during clustering analysis. The stability of a cluster can be determined from its binding energy $E_{Binding}$, which is the difference in energy between the cluster $E_{Cluster}$ and the sum of its constituent point defects E_{Defect}, as shown in equation 7.

$$E_{Binding} = E_{Cluster} - \sum E_{Defect} \tag{7}$$

For example, the binding energy of a $2Nd^{\bullet}_{Cd}{:}O''_i$ cluster is calculated following equation 8.

$$E_{Binding} = E(2Nd^{\bullet}_{Cd}O''_i) - E(O''_i) - 2E(Nd^{\bullet}_{Cd}) \tag{8}$$

A negative binding energy would indicate that the cluster is bound, and, is more favourable compared to the defects at infinite separation.

As previously discussed, an oxygen interstitial is formed for every two dopants in order to maintain charge neutrality. Therefore, the simplest charge neutral defect cluster would consist of a single oxygen interstitial and a pair of neighbouring dopant ions ($2M^{\bullet}_{Cd}{:}O''_i$). Investigation of small $2M^{\bullet}_{Cd}{:}O''_i$ clusters can be conducted with relative ease due to the limited number of possible permutations ($\sim$4000). The complex nature of defect clustering means behaviours may differ in larger clusters. However investigation of larger clusters quickly becomes infeasible due to the vast number of possible conformations associated with them ($> 1 \times 10^7$ for $4M^{\bullet}_{Cd}{:}2O''_i$ systems). As such, investigations have been restricted to $2M^{\bullet}_{Cd}{:}O''_i$ clusters. Any effects which may arise from further clustering will be captured during the molecular dynamics simulations where the random placements of clusters lead to finding some in proximity to one another. With the exception of Y, each dopant is found to present only a single stable $2M^{\bullet}_{Cd}{:}O''_i$ cluster conformation. The Sc and Y based clusters adopt "Ge_3O_{13}" based defect structures, as shown in figure 3a, in which the dopants, like the natural Cd ions, are six coordinate. However, the "GeO_5" structure shown in figure 3b is favoured by the three larger dopants, Nd, Pr and La, as it affords them a more preferable seven coordinate environment. The existence of interstitially bridged defects has been proposed in other materials such as "Ge_2O_9" groups in apatite.[2,31] However, currently, no reports of analogous "Ge_3O_{13}" type defect structures can be found.

Table 4 Corrected solution energies for the trivalent doping of Cd_2GeO_4 *via* the mechanism detailed in equation 3.

Dopant	Radii (Å)	$E_{Solution}$ (eV)
Sc	0.75	1.06
Y	0.9	0.60
Nd	0.98	0.11
Pr	0.99	0.09
La	1.03	0.09
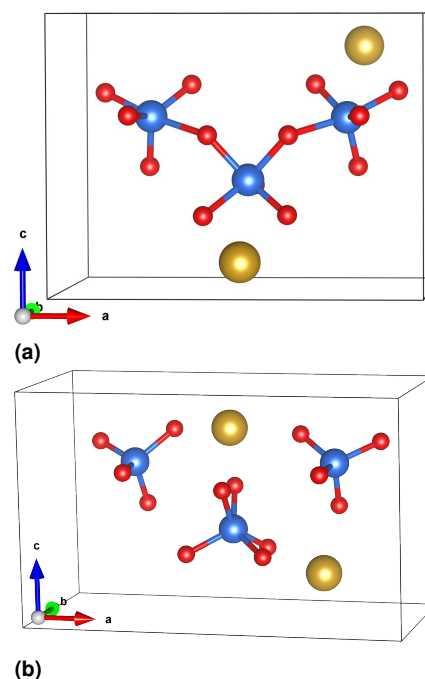
Fig. 3 a) "Ge_3O_{13}" and b) "GeO_5" $2M^{\bullet}_{Cd}{:}O''_i$ clusters, with O, Ge and M represented as red, blue and gold spheres respectively. Surrounding ions omitted for clarity.

The calculated binding energies for the stable $2M^{\bullet}_{Cd}{:}O''_i$ defect clusters are reported in table S1 and are plotted against dopant size in figure 4a. Examination reveals defect clustering to be a highly favourable process. Therefore, the existence of isolated defects, particularly at non-trivial defect concentrations, is unlikely. Furthermore, the binding energy generally decreases as the dopant's radius deviates from the native Cd ion's (0.95 Å), which is due to the dopant size dependency of the lattice relaxation interactions (discussed later). As the previously discussed solution energies were calculated assuming infinite dilution they failed to take into account the additional stabilisation energy arising from defect-defect interactions. This results in an overestimation of the solution energies due to the non-trivial nature of such interactions. However, this can be corrected for by simply adding the binding energy to the solution energy. It can be seen from table 4 that dopant incorporation is much more favourable once defect-defect stabilisation energy is factored in.

Although binding energies are an approximate indicator due to their complicated nature of the extent to which an oxygen interstitial may become trapped, it is more appropriate to consider
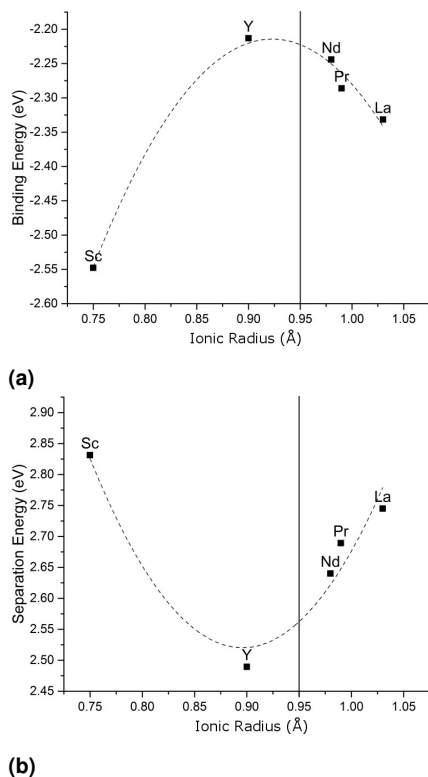
Fig. 4 a) Binding and b) interstitial separation energies of $2M^{\bullet}_{Cd}$:O''_i clusters as a function of dopant radius with Cd's ionic radius indicated by the solid black line, trend line include as a guide only.

interstitial separation energy. This represents the energy required to remove an oxygen interstitial from its cluster to infinity. The separation energy is calculated as the difference in binding energy between a cluster with and without its oxygen interstitial. The calculated interstitial separation energies for the $2M^{\bullet}_{Cd}$:O''_i clusters are presented in table S1 and figure 4b. Again, this shows increased separation energies for dopants notably larger or smaller than Cd. The larger the dopant ion the greater its preference for the seven coordinate environment provided by the oxygen interstitial. Small dopants, such as Sc, are a poor fit for the native Cd site. However, interstitial defects allow the oxygen ions to relax around to dopant to accommodate it better. As such, the energetic penalty for the movement of an oxygen interstitial away from its $2M^{\bullet}_{Cd}$:O''_i cluster is likely to be greater for dopants notably larger or smaller then Cd. This suggests that ions closer in size to Cd are generally more appropriate dopants, as their lower trapping capability suggests increased oxide defect mobility. However, this is not conclusive as it fails to provide information on the short to medium range defect interactions. Further to this, molecular dynamic simulations were carried out to elucidate interstitial defect trapping at higher temperatures. This being said, the large binding and separation energies clearly show that interstitial diffusion will be heavy restricted by the dopants with a high trapping probability.

3.4 Diffusion

Molecular dynamic simulations were conducted on pristine and 10% doped Cd_2GeO_4 in order to assess the impact of doping on oxide ion conduction. Yttrium was selected as the primary dopant due to its reduced binding and separation energies. The starting structures for the doped systems were generated by randomly placing 25 $2M^{\bullet}_{Cd}$:O''_i clusters in 5×5×5 supercells.
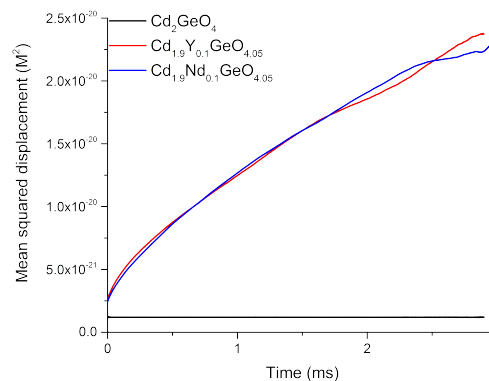

Fig. 5 Mean squared displacements for oxygen in Cd_2GeO_4 (black), $Cd_{1.9}Y_{0.1}GeO_{4.05}$ (red) and $Cd_{1.9}Nd_{0.1}GeO_{4.05}$ (blue) at 1273 K MD simulations.

The mean squared displacements (MSD) of the oxide ions, figure 5, clearly shows oxygen diffusion is only significant in doped systems. The diffusion coefficients for oxygen in $Cd_{1.9}Y_{0.1}GeO_{4.05}$, as calculated following equation 2, are presented in figure 6 table S2. The MD results suggest that, although mobile, the oxide defects generally reside in the dopant rich regions of the cell, shown from the O-Y and O-Cd_{II} radial distribution functions presented in figure 7. This supports the earlier defect clustering analysis which indicated trapping of the interstitials by the dopants to be highly favourable. As previously discussed $2Y^{\bullet}_{Cd}$:O''_i clusters assume "Ge_3O_{13}" based structures while larger ions such as Nd prefer to adopt "GeO_5" based clusters. To probe the effects of differing defect cluster structures on oxide diffusion a limited number of simulations were conducted on Nd doped Cd_2GeO_4 systems. The diffusion coefficients for the Nd doped systems were found to be comparable to those of Y doped systems, as indicated by the MSDs in figure 5. This suggests that the difference in interstitial trapping of the Y and Nd doped systems, calculated at high temperature, is negligible compared to their overall binding energies which were calculated at zero kelvin.

The calculated diffusion coefficients are found to be several orders of magnitude higher than those of the common cathode material LSM-20 and on a par with composite cathode materials such as YSZ-40 wt.% LSM which, at 1073 K, have diffusion coefficients of 1.3×10^{-12} and 1.0×10^{-9} cm^2 s^{-1} respectively.[32] However, many common electrolyte or advanced electrode materials present significantly higher diffusion coefficients, for example yttria stabilized zirconia (2.6×10^{-7} cm^2 s^{-1} at 1273 K) and lanthanum strontium cobalt ferrite (2.6×10^{-9} cm^2 s^{-1} at

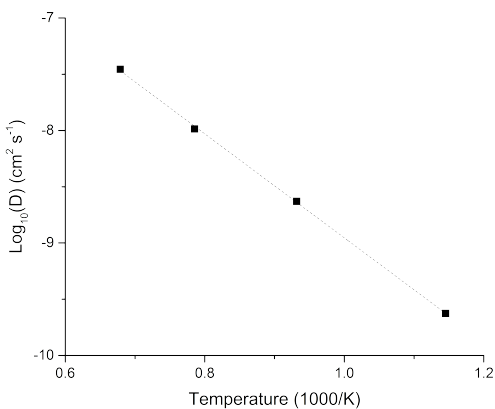**Fig. 6** Plot showing temperature dependency of oxygen diffusion in $Cd_{1.9}Y_{0.1}GeO_{4.05}$.

773 K).[23,29]

The MD results suggest that oxide ions diffuse primarily in the ac-plane, which is shown by the axial MSDs (figure S1), with a calculated activation energy of 0.92 eV, and that, like apatite germinates, all oxide ions are found to be mobile.[2] The oxide defects diffuse down the a-axis through the sequential formation of "Ge_3O_{13}" and intermediary "Ge_2O_9" defects between nearest neighbouring tetrahedra in a "knock-on" type mechanism. This mechanism, which is depicted in figure 8, forms diffusion channels along to the a-axis as represented in figure 9. This bears a striking resemblance to the oxygen vacancy diffusion mechanism reported in $La_{1-x}Ba_{1+x}GaO_{4-x/2}$.[33] Movement between these channels is permitted by the c-axial diffusion mechanism. This mechanism differs from the former in that it is stepwise and as oxide ions must unbind from their tetrahedra, traverse the Cd_{II} channel and rebind with another tetrahedra. The exact pathway of this mechanism is highly dependent on the local environment, specificity the presence of dopant or other interstitial ions. Similar anisotropic diffusivity is predicted via static lattice methods for olivine (Mg_2SiO_4) itself. Such work reports a-axial diffusion is also favoured, with an activation energy of 0.97 eV.[20]
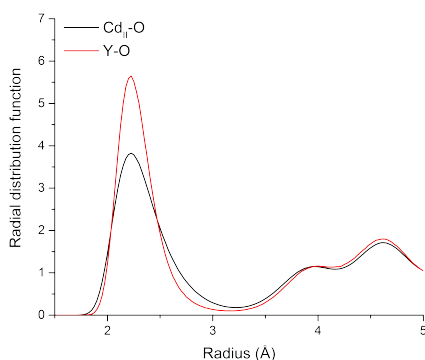

Fig. 7 Radial distribution functions for O about Cd_{II} and Y at 1473 K.

4 Conclusion

To summarise, in this work we predict that oxygen defect formation in olivine-type Cd_2GeO_4 can be promoted through trivalent doping which follows a constant-cation mechanism. Furthermore, the dopant ion, and the size thereof, is predicted to play a significant role in trapping the mobile defects (a complicated phonomenon to capture fully in a computational model). The oxide ion interstitial diffusion primarily occurs in the ac-plane via a "knock-on" mechanism along a-axis, in line with previous migration pathways reported in the Li - olivine structure and via a stepwise mechanism along the c-axis. However for the first time we explicitly show, that even at high temperatures the mobile oxide ions tend to stay within the dopant rich regions of the cell. Thus confirming the favourability of dopant trapping, which partially inhibits oxide ion transport. Finally, from our MD simulations we calculated migration barriers of 0.92 eV. In conclusion, whilst trivalent doping on the Cd site shows some promise, the oxide ion trapping capabilities of the dopant ions limit the use of Cd_2GeO_4 as an oxide ion conductor. Finally, we show the use of simulations to illustrate the potential of the olivine structure to accommodate interstitial oxide ions, and exclusively quantify the binding energies and, hence, the trapping of such mobile defects in this material. In addition to the relevance in the oxide ion conductor field, this work is also of relevance to the Li ion battery field, given the large interest in olivine-type $LiFePO_4$.

References

1 N. Mahato, A. Banerjee, A. Gupta, S. Omar and K. Balani, *Prog. Mater. Sci.*, 2015, **72**, 141–337.

2 E. Kendrick, M. S. Islam and P. R. Slater, *Chem. Commun. (Camb).*, 2008, **33**, 715–717.

3 J. R. Tolchard, M. S. Islam and P. R. Slater, *J. Mater. Chem.*, 2003, **13**, 1956–1961.

4 P. R. Slater, J. E. H. Sansom and J. R. Tolchard, *Chem. Rec.*, 2004, **4**, 373–384.

5 P. M. Panchmatia, A. Orera, G. J. Rees, M. E. Smith, J. V. Hanna, P. R. Slater and M. S. Islam, *Angew. Chemie Int. Ed.*, 2011, **50**, 9328–9333.

6 X. Kuang, M. A. Green, H. Niu, P. Zajdel, C. Dickinson, J. B. Claridge, L. Jantsky and M. J. Rosseinsky, *Nat. Mater.*, 2008, **7**, 498–504.

7 M. S. Islam, D. J. Driscoll, C. A. J. Fisher and P. R. Slater, *Chem. Mater.*, 2005, **17**, 5085–5092.

8 E. Whipple, S. Subbarao and F. Koffyberg, *J. Solid State Chem.*, 1980, **34**, 231–239.

9 A. K. Cheetham and P. Day, *Solid State Chemistry: Techniques*, Clarendon Press, 1988.

10 A. R. Leach, *Molecular Modelling: Principles and Applications*, Prentice Hall, 2001.

11 C. R. A. Catlow, *Computer Modeling in Inorganic Crystallography*, Elsevier Science, 1997.

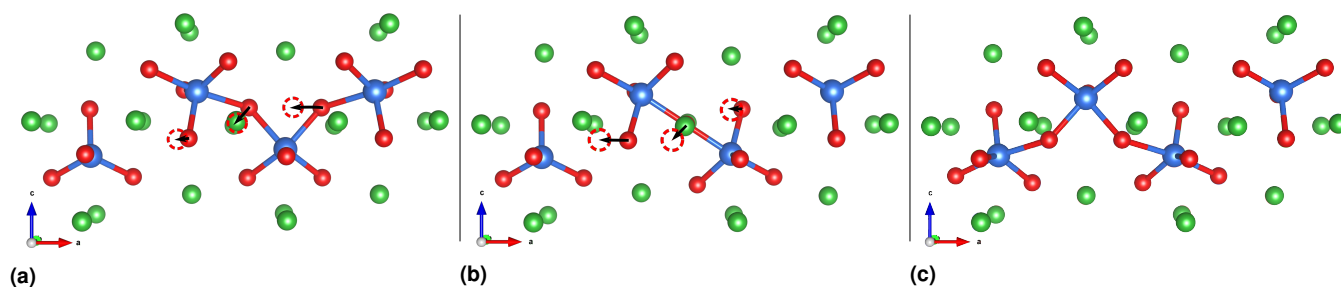12 J. D. Gale, *J. Chem. Soc. Faraday Trans.*, 1997, **93**, 629–637.

Fig. 8 Schematic representation of oxygen defect migration along the *a*-axis via the formation and breaking of an intermediary "Ge_2O_9" group. With Ge, Cd and O ions represented as blue, green and red spheres respectively.
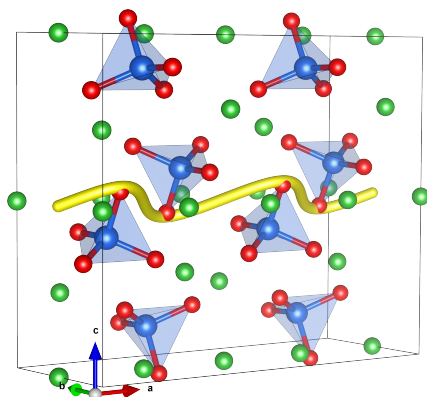

Fig. 9 Depiction of the primary *a*-axial diffusion pathway (yellow) elucidated from 1273 K MD simulations of $Cd_{1.9}Y_{0.1}GeO_{4.05}$. With Ge, Cd and O ions represented as blue, green and red spheres respectively.

13 J. D. Gale and A. L. Rohl, *Mol. Simul.*, 2003, **29**, 291–341.

14 W. Smith and T. R. Forester, *J. Mol. Graph.*, 1996, **14**, 136–141.

15 K. Momma and F. Izumi, *J. Appl. Crystallogr.*, 2011, **44**, 1272–1276.

16 R. A. Buckingham, *Proc. R. Soc. Lond. A. Math. Phys. Sci.*, 1938, **168**, 264–283.

17 M. A. Simonov, E. L. Belokoneva and N. V. Belov, *J. Struct. Chem.*, 1981, **22**, 478–479.

18 B. G. Dick and A. W. Overhauser, *Phys. Rev.*, 1958, **112**, 90–103.

19 N. F. Mott and M. J. Littleton, *Trans. Faraday Soc.*, 1938, **34**, 485–499.

20 A. M. Walker, K. Wright and B. Slater, *Phys. Chem. Miner.*, 2003, **30**, 536–545.

21 P. M. Panchmatia, A. Orera, E. Kendrick, J. V. Hanna, M. E. Smith, P. R. Slater and M. S. Islam, *J. Mater. Chem.*, 2010, **20**, 2766–2772.

22 J. R. Tolchard, P. R. Slater and M. S. Islam, *Adv. Funct. Mater.*, 2007, **17**, 2564–2571.

23 C. Sun, R. Hui and J. Roller, *J. Solid State Electrochem.*, 2010, **14**, 1125–1144.

24 C. Fisher, M. Islam and R. Brook, *J. Solid State Chem.*, 1997, **128**, 137–141.

25 S. J. Skinner and J. A. Kilner, *Mater. Today*, 2003, **6**, 30–37.

26 Y. Jin, Y. Hu, R. Chen, Y. Fu, G. Ju, Z. Mu, J. Lin, Z. Wang, F. Xue and Q. Zhang, *J. Alloys Compd.*, 2015, **623**, 255–260.

27 W. Haynes, *CRC handbook of chemistry and physics : a ready-reference book of chemical and physical data*, CRC Press, Boca Raton, FL, 2011.

28 B. Wang, R. J. Lewis and A. N. Cormack, *Acta Mater.*, 2011, **59**, 2035–2045.

29 R. Devanathan, W. J. Weber, S. C. Singhal and J. D. Gale, *Solid State Ionics*, 2006, **177**, 1251–1258.

30 M. Schie, R. Waser and R. A. De Souza, *J. Phys. Chem. C*, 2014, **118**, 15185–15192.

31 K. Imaizumi, K. Toyoura, A. Nakamura and K. Matsunaga, *Solid State Ionics*, 2014, **262**, 512–516.

32 S. Jiang, *J. Mater. Sci.*, 2008, **43**, 6799–6833.

33 E. Kendrick, J. Kendrick, K. S. Knight, M. S. Islam and P. R. Slater, *Nat Mater*, 2007, **6**, 871–875.

34 M. Levy, *PhD thesis*, Imperial College London, 2005.

35 L. Minervini, R. W. Grimes and K. E. Sickafus, *J. Am. Ceram. Soc.*, 2000, **83**, 1873–1878.

Physical Chemistry Chemical Physics Accepted Manuscript